Advanced Laboratory Course
E207: Lab Course Accelerator Bonn (LAB)

Amelia Carina de Lope Fend, Martin Ludwig

26.02.2025

Contents

1. Introduction

Particle accelerators are the foundation of modern scattering experiments and therefore enable physicists to study the structure of matter on its smallest scales. Besides their applications in physics, accelerators are also indispensable in contemporary medicine and materials science. In addition to acceleration, the most important task of an accelerating machine is to steer the beam, that is, to keep it focused and on its intended orbit.

In this experiment, we study the beam steering using a 25 keV linear accelerator for electrons. Our aim is to adjust multiple corrector and quadrupole magnets so that the electron beam is well-aligned and focused. After that, the beam emittance, which is a measure of its spread, is to be measured using two different methods.

This report is structured as follows: Chapter 2 introduces the experimental setup and explains the different components of the accelerator. After that, the measurements and their analysis are described in Chapter 3. In Chapter 4, the results are summarized.

2. Experimental Setup

The experiment was conducted with the 25 keV LAB accelerator whose structure and components are introduced in the following section. All presented information was taken from [1].

The LAB beamline (see Figure 2.1) can basically be divided into two parts. The first part contains a gun, in which electrons are emitted and accelerated, two solenoids for basic focusing, and a corrector magnet for beam alignment. The second part consists of four structurally identical sections, each including a screen, a quadrupole magnet, and a corrector magnet. The screens are used to monitor the beam position and profile, the quadrupoles focus the beam, and through the corrector magnets a so-called kick can be applied to center the beam inside the beam pipe. Every part of the accelerator can be controlled with the LAB control system installed on a computer in the lab room. In particular, the strengths of all magnets can be set there, and the images from the screens can be displayed.

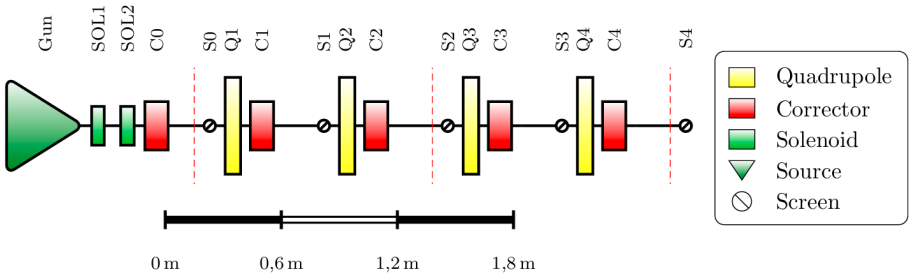

Figure 2.1.: Overview of the LAB accelerator and its components. Figure taken from [1].

In the following subsections, the aforementioned components are described in more detail.

2.1. Electron Gun

The purpose of the gun is to produce and accelerate the electron beam. Initially, electrons are emitted from a filament via the thermionic effect. A thin wire made of a material with a relatively low work function is used for the filament (YO_xIr, $W_e \approx 2.6\,\mathrm{eV}$), so that electrons can easily leave it when the material is heated by an electric current. Since the electrons are emitted isotropically, they must be focused to form a beam. This focusing is achieved by a (relative to the filament) negatively charged Wehnelt cylinder, which provides a radial electric field that pushes the electrons toward its center. The electrons exit the cathode through a hole, along which they are accelerated by a relatively small initial acceleration voltage (see Figure 2.2)

The entire cathode is held at a potential of $-25\,\mathrm{kV}$ and is isolated from the anode and the subsequent beamline, which are at ground potential. Consequently, the electrons leaving the

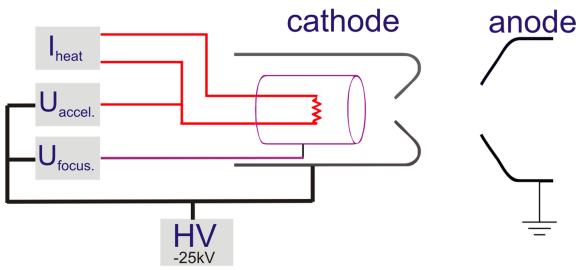

Figure 2.2.: Schematic drawing of the electron gun and its wiring. Figure taken from [1].

cathode hole are strongly accelerated toward the anode and eventually reach a velocity of approximately $0.3c$. The cathode and anode are shaped so that the electric field lines have a radial component, contributing to the beam focusing. In order to prevent collisions with gas molecules, the entire beam pipe is evacuated, with a slightly better vacuum ($\sim 10^{-8}$ mbar) in the electron gun compared to the rest of the accelerator ($\sim 10^{-7}$ mbar).

2.2. Magnets

According to the Lorentz force, magnetic fields bend the trajectories of moving charged particles. Following this principle, different kinds of magnets are used to steer and focus the beam in an accelerator.

Some initial focusing can be achieved using **solenoids**, which are cylindrical coils that provide a longitudinal magnetic field. They cause electrons with a transverse momentum component to follow helical orbits and focus them via their fringe fields.

Corrector magnets are used to deflect the beam horizontally or vertically. This is required because even a perfectly aligned beam in an ideal accelerator would experience some bending due to Earth's magnetic field, which must be compensated to keep the beam on a straight path. Corrector magnets are designed to deflect the beam by a small "kick" angle α, which depends on the charge of the beam particles (in our case, for electrons, simply e), their momentum p, as well as the corrector's length L and its magnetic field B:

$$\alpha \approx \frac{eBL}{p}$$

Here, L refers to the effective length of the magnet, which generally differs from its physical length. It is introduced to account for the non-ideal, inhomogeneous field of a real magnet and is defined as the length that an ideal magnet without any fringe fields would need to produce the same integrated B field.

Practically, for the corrector magnet in the experiment, two perpendicular pairs of coils are used. They are placed in a Helmholtz configuration to achieve an almost homogeneous magnetic field, and they can be adjusted independently to enable beam deflection in both the horizontal and vertical directions. Each corrector can be actuated via the LAB control system, which regulates the magnets' currents so that the set deflection angle is applied.

The purpose of **quadrupole magnets** is to focus the beam. Focusing is necessary because, due to electric repulsion, an initially small beam tends to drift apart. As its name implies, a quadrupole has four pole shoes, forming two north and two south poles. They are arranged such that like poles face each other (see Figure 2.3). This design creates a magnetic field that is strongest at the rim and vanishes at the center of the quadrupole. Therefore, beam particles passing through the quadrupole's center are not affected by it, while displaced particles are deflected according to the Lorentz force. This deflection occurs in opposite directions for horizontally and vertically displaced particles, meaning that a quadrupole can only focus in one plane. That is why accelerators employ quadrupoles that focus alternately in the horizontal and vertical planes.

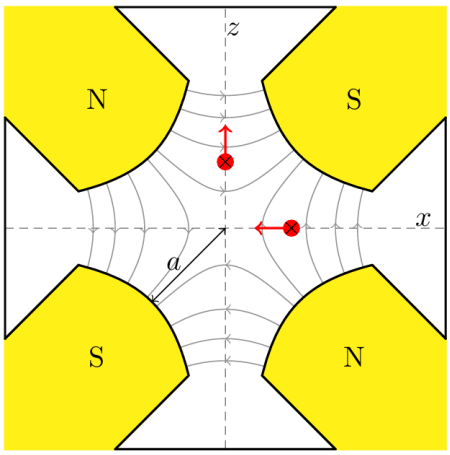

Figure 2.3.: Structure and functional principal of a quadrupole magnet. The red arrows indicate the Lorentz force acting on a horizontally and vertically displaced electron flying into the drawing plane. Figure taken from [1].

To quantify the focusing of a quadrupole, one defines the quadrupole strength

$$k = \frac{e}{p} \cdot \frac{2\mu_0 n I}{a^2},$$

where we assume a beam particle with charge e and momentum p, μ_0 denotes the vacuum permeability, n is the number of coil windings, I is the current, and a is the quadrupole's half aperture (see Figure 2.3). Since all other parameters in this formula are fixed for this experiment, the quadrupole strength depends only on the applied current, which can be set in the LAB control system. Using the known values for the physical constants, the momentum ($p = \sqrt{E^2 - m_e^2} \approx E = 25\,\mathrm{keV}$), the number of windings ($n = 120$) and the half aperture ($a = 28\,\mathrm{mm}$), the software directly translates a set current into the corresponding value of k.

2.3. Screens

To be able to reasonably adjust the correctors and quadrupoles, it is necessary to know the beam position and profile along the accelerator. For this purpose, five screens are available

that can be moved into the beam pipe. They are oriented at a 45° angle to the beam line and are covered with aluminium oxide, which fluoresces after being hit by the electron beam. Due to the 45° angle, the fluorescence light is emitted perpendicular to the beam pipe and recorded by a CCD camera. The image is then digitized and displayed on the lab computer's monitor. The display software also fits a two-dimensional Gaussian curve to the beam profile to determine the beam position relative to the center as well as its spread (corresponding to the standard deviation of the Gaussian function).

3. Measurements and Analysis

The measurements we perform in this experiment can be divided into two main parts. In the first part, the calibration of the corrector magnets is verified (Section 3.1) and the beam is aligned (Section 3.2). This includes adjusting all corrector magnets so that the beam passes through the center of the quadrupoles, as well as adjusting the quadrupoles so that the beam is well-focused. In the second part, the emittance of the electron beam is measured via the quadrupole scan method (Section 3.4) and the multi-screen method (Section 3.5).

3.1. Verification of the Corrector Magnet Calibration

3.1.1. Method

Before aligning the beam, the calibration of the kick angle of the corrector magnets is to be checked. This refers to the relation of the kick angle α and the resulting displacement from the design trajectory x after a certain drift length L. We assume small angles α, therefore

$$\frac{x}{L} = \tan\alpha \approx \alpha \tag{3.1}$$

should hold true. Here and in what follows, we use x to denote the horizontal displacement, with the same relation holding for vertical displacements z. For convenience, only the formulas for x are stated.

3.1.2. Measurement

We can check relation 3.1 by measuring the displacement x at different angles α, which we can set by varying the corrector current I^C. This is done for two pairs of corrector magnets and screens, C0 and S0 as well as C1 and S1, in both the vertical and horizontal planes. The quadrupole magnet Q1 is turned off during this part. We estimated the uncertainty of the displacement based on the range over which it fluctuates during the measurements. For the angle, we assume a constant error of 0.1 mrad. The resulting values can be found in Table A.1 and Table A.3 in the Appendix.

3.1.3. Fitting the Measurements

As we expect a linear dependency, we fit the data with a function

$$x(\alpha) = m \cdot \alpha + n. \tag{3.2}$$

When the magnets are turned off, the beam does not necessarily pass through the center of the screens due to Earth's magnetic field and possible initial misalignments. Therefore, the offset n is arbitrary. m should correspond to the drift length L, if the corrector magnets are

calibrated sufficiently well. The drift length can be deduced from the individual component lengths given in the script. This includes half the length of the corrector magnet, the drift length between the corrector magnet and the screen, and, due to the angled position of the screen, half the screen length. This yields:

$$L_{C0\to S0} = 244.25\,\text{mm} \qquad L_{C1\to S1} = 375.25\,\text{mm} \tag{3.3}$$

The fit results are displayed in Figures 3.1 and 3.2. In addition to the measurements, green lines are plotted which were obtained by substituting the actual lengths from Eq. 3.3 as the slopes. It is striking that the measured values consistently exhibit a steeper slope than the green lines, which is equivalent to the experimentally determined lengths (284(2) mm and 306(2) mm for $L_{C0\to S0}$ as well as 462(9) mm and 520(22) mm for $L_{C1\to S1}$) being significantly larger than the actual lengths from Eq. 3.3. This suggests a systematic error or an actual miscalibration of the corrector magnets.

Furthermore, the small error bars and correspondingly large χ^2/ndf values indicate that we have underestimated the uncertainties in the beam positions. We conclude that the range over which the beam position values fluctuate is not a good estimator of their actual uncertainty. Rather, we must assume that the implicit assumption of a Gaussian profile, the relatively large beam spread (compared to the range over which the peak position fluctuates), and a possibly imperfect alignment of the screens introduce additional errors that, in sum, are significantly larger than the uncertainties we have estimated.

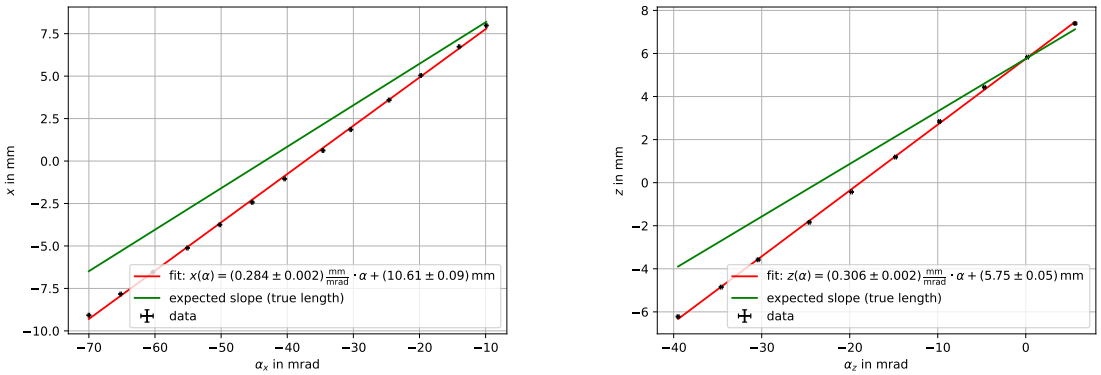

(a) Horizontal direction. $\chi^2/\text{ndf} = 43.86$ (b) Vertical direction. $\chi^2/\text{ndf} = 16.64$

Figure 3.1.: Verification of the calibration of C0: Displacements as a function of the applied angle α.

Despite the partly large differences between the slopes of the red and green lines, we can conclude that all plots clearly show the expected linear relationship between the set angle and the resulting deflection. Since only this fact is important for the subsequent beam alignment, the potentially faulty corrector calibration has no negative impact on the further course of the experiment.

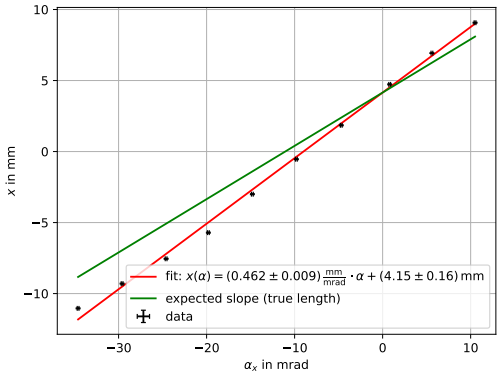

(a) Horizontal direction. $\chi^2/\text{ndf} = 218.74$

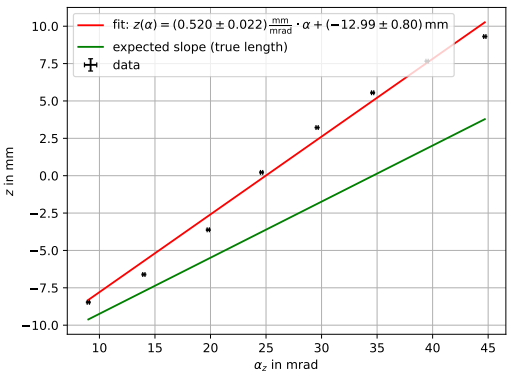

(b) Vertical direction. $\chi^2/\text{ndf} = 1002.20$

Figure 3.2.: Verification of the calibration of C1: Displacements as a function of the applied angle α.

3.2. Beam-based Alignment

3.2.1. Procedure for the Beam Alignment

The goal of this part is to align the beam such that it passes through the center of each quadrupole magnet. This is necessary to ensure that the quadrupoles only focus the beam and do not additionally deflect it. For the so-called beam-based alignment, we follow the procedure outlined below:

1. First, we adjust corrector C0 so that the beam hits the center of screen S0. Since screen S0 is located relatively close to quadrupole Q1, this already provides a rough estimate for the required corrector current I^C.

2. Next, with quadrupole Q1 turned off, we observe the beam on screen S1 and adjust corrector C1 so that the beam appears centered on S1.

3. Then we turn on quadrupole Q1 and observe how the beam position on screen S1 changes. We take advantage of the fact that if the beam is perfectly centered in the quadrupole, its position should not change, and we search for two quadrupole strengths k at which the beam position on screen S1 is clearly distinct. The LAB control system allows us to switch back and forth between these two k values at regular intervals.

4. Now we return to C0 and adjust the kick angle in the x- and z-directions until the beam on S1 no longer changes its position. Once this is the case, the ideal setting for corrector C0 has been found.
   We initially perform this step by eye in order to get a sense of where the ideal setting approximately lies. Then we choose five corrector currents I^C near these visually determined ideal value and, for each I^C, measure the two beam positions $x(k_1)$ and $x(k_2)$ (or $z(k_1)$ and $z(k_2)$). The ideal setting occurs when the difference $\Delta x = x(k_1) - x(k_2) = 0$ (or, analogously, $\Delta z = z(k_1) - z(k_2) = 0$) and is determined by a linear fit. We then set the resulting fit value on C0 and do not adjust it further.

5. Finally, the entire procedure is repeated for the other corrector magnets C1, C2, and C3, each time using the corresponding screens and quadrupoles.

3.2.2. Fitting the Measurements

The fit used to determine which current corresponds to a displacement of zero is a linear one:

$$\Delta x(I^C) = a \cdot I^C + b \tag{3.4}$$

Again, the same applies for z but we only state the formulas for x. The current for which the displacement Δx vanishes corresponds to the root of the fitted function and can be calculated via

$$I_0^C = -\frac{b}{a}.$$

While reading off the displacement values, we observed constant fluctuations. We take the maximum deviation from the measured value as its error. For the corrector current, we

estimated a constant uncertainty of 0.5 mA. The values for these measurements can be found in the Appendix in Tables A.5 to A.11.

Figures 3.3 to 3.6 show all the linear fits for the corrector magnets C0 to C3, and Table 3.1 displays the corresponding ideal values for the corrector currents (i.e., the roots of the fit functions). All plots clearly demonstrate the expected linear relationship between the corrector current and the difference in beam deflections. Through the initial adjustment per eye, some measurement points could always be placed below and above the expected minimum, allowing us to determine the zeros with good accuracy. In most cases, the calculated zeros deviated only slightly from those determined visually.

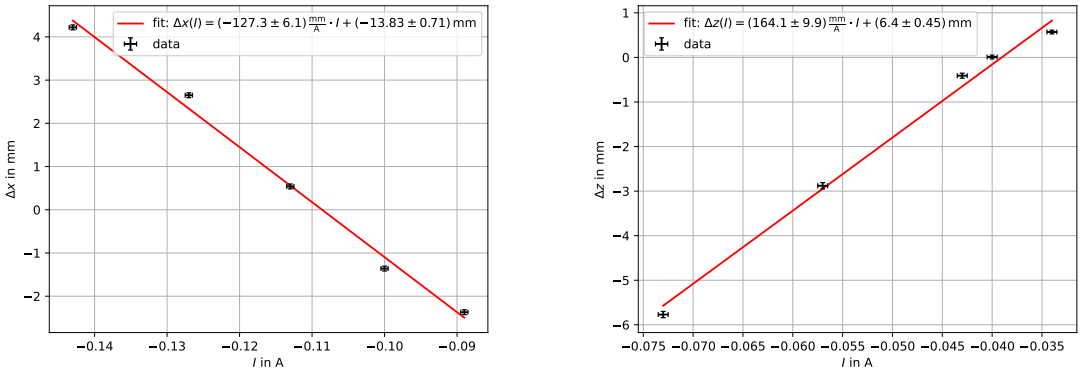

(a) Horizontal direction. $\chi^2/\text{ndf} = 21.49$ (b) Vertical direction. $\chi^2/\text{ndf} = 26.32$

Figure 3.3.: Beam-based alignment for the corrector magnet C0: Displacement differences as a function of the corrector current I^C.

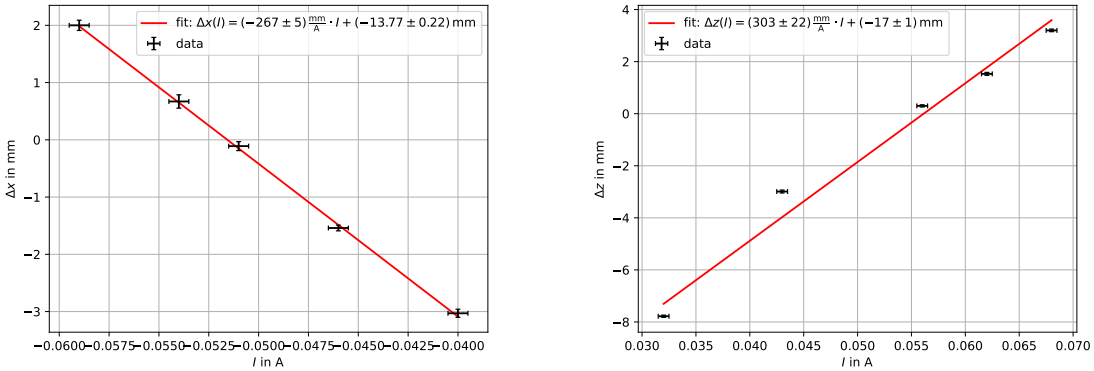

(a) Horizontal direction. $\chi^2/\text{ndf} = 0.72$ (b) Vertical direction. $\chi^2/\text{ndf} = 191.15$

Figure 3.4.: Beam-based alignment for the corrector magnet C1: Displacement differences as a function of the corrector current I^C.

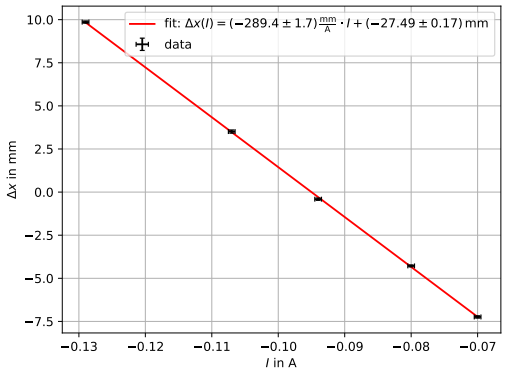

(a) Horizontal direction. $\chi^2/\text{ndf} = 1.55$

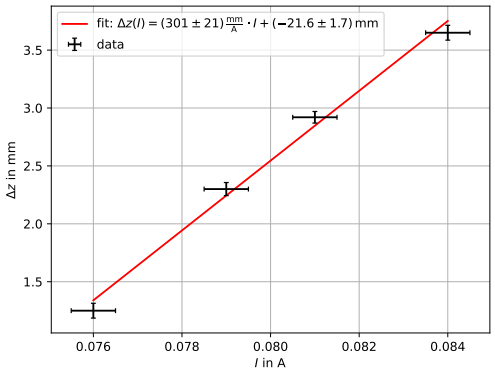

(b) Vertical direction. $\chi^2/\text{ndf} = 3.79$

Figure 3.5.: Beam-based alignment for the corrector magnet C2: Displacement differences as a function of the corrector current I^C.

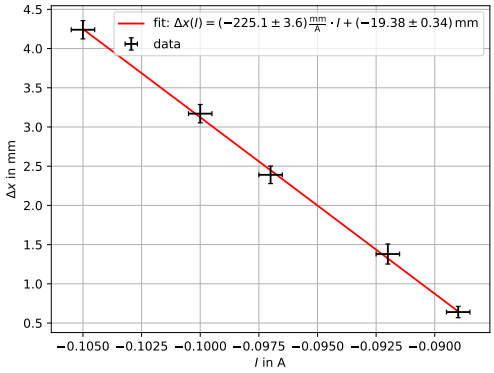

(a) Horizontal direction. $\chi^2/\text{ndf} = 0.22$

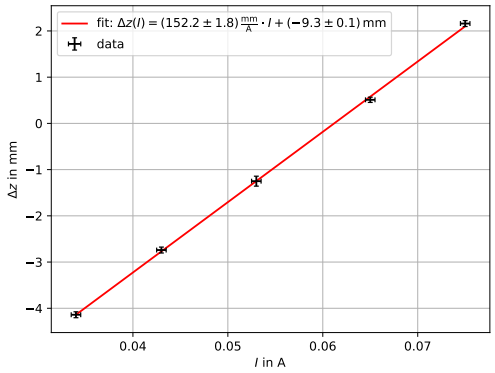

(b) Vertical direction. $\chi^2/\text{ndf} = 0.85$

Figure 3.6.: Beam-based alignment for the corrector magnet C3: Displacement differences as a function of the corrector current I^C.

Table 3.1.: Ideal currents I_0^C for all corrector magnets (corresponding to the roots of the determined fit functions).

	C0	C1	C2	C3
x	$-0.109(8)$	$-0.052(1)$	$-0.095(1)$	$-0.086(2)$
z	$-0.039(4)$	$0.056(6)$	$0.072(8)$	$0.061(1)$

Our error estimation appears to be plausible in most cases, as the χ^2/ndf values indicate. Only for the vertical adjustment of corrector C1 (see Fig. 3.4b) the quality of the fit is noticeably poor. This is probably because for the first measurement a beam position

relatively close to the edge of the screen was used, so the beam center was likely determined with low accuracy.

After setting each corrector current according to Table 3.1, we once again used the toggle mode for the quadrupole magnets to check whether the beam still jumped when the quadrupole strength was changed. In all cases, the shape changed, but the center's position remained the same. Therefore, as far as we could tell, the beam was properly aligned after this procedure. Finally, we adjusted the quadrupole strengths with the aim of achieving the most focused result. While doing so, we ensured that the quadrupole strengths of two consecutive quadrupoles had opposite signs, thereby focusing the beam in each direction.

3.2.3. Beam Profiles

Figure 3.7 shows the beam profile after alignment on all five screens. After an odd number of quadrupole magnets, that is, on screens S1 and S3, the beam profile resembles an ellipse more than a circle. This is because an even number of quadrupoles is required to achieve equal focusing in both directions, as each quadrupole only focuses in one direction. As a result, one direction is more focused than the other, leading to an elliptical shape. On screens S1 and S2, the beam is intense and appears well focused; on the following screens, S3 and S4, the beam shape is broader and thus not as well focused.

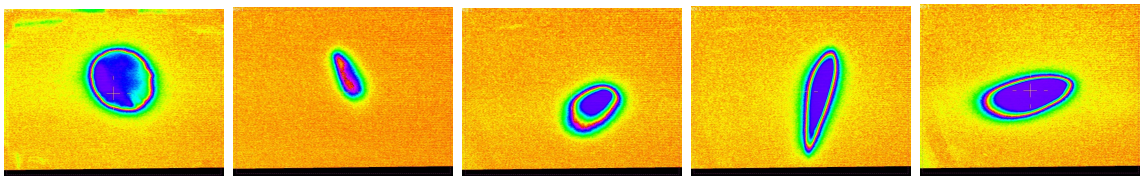

Figure 3.7.: The beam profile on screens S0, S1, S2, S3 and S4 (from left to right) after the beam alignment procedure.

3.3. Linear Beam Dynamics

Before evaluating the remaining parts of the experiment, it is necessary to introduce some theoretical accelerator physics concepts. This will provide more context for the quantities and relations used when analyzing the measurements. All of the presented information was taken from [1].

3.3.1. Hill's Equation

The first of these concepts is the curvilinear coordinate system used to describe a particle's trajectory. A particle's position in this system is given by the three coordinates x, z, and s. Here, s denotes the trajectory of an ideal design particle, while x and z represent the deviations of a particle from this design trajectory in the horizontal and vertical directions, respectively. Dipole magnets bend the trajectory with a local bending radius $R(s)$, and quadrupole magnets focus the beam with a quadrupole strength $k(s)$. It can be shown that the motion of a particle in an accelerator is described by Hill's differential equations:

$$x''(s) + \left(\frac{1}{R^2(s)} - k(s)\right) \cdot x(s) = \frac{1}{R(s)} \frac{\Delta p}{p} \tag{3.5}$$

$$z''(s) + k(s) \cdot z(s) = 0 \tag{3.6}$$

Here p is the particle's momentum and Δp is the momentum spread. For a linear accelerator, the bending radius is infinite resulting in a simplified equation for $x''(s)$. These equations are solved by pseudoharmonic oscillations. This refers to an oscillation around the design trajectory, where the amplitude $A(s)$ and the phase, which is composed of an initial phase ϕ and the phase advance $\psi(s)$, depend on the coordinate s. Thus the motion of an individual particle in, for example, the horizontal plane is described by

$$x_i(s) = A_{x,i}(s) \cos\left(\Psi_x(s) + \phi_i\right). \tag{3.7}$$

3.3.2. Matrix Formalism

Analogous to the matrix formalism in geometrical optics, the influence of a magnet or a drift on a particle's displacement can be expressed using a matrix representation. For this purpose, we introduce the vector

$$\vec{x} = \begin{pmatrix} x \\ x' \end{pmatrix},$$

which contains the horizontal displacement x and its angle $x' = \frac{\mathrm{d}x}{\mathrm{d}s}$. A similar representation can be defined for the vertical displacement z, resulting in the four-dimensional vector

$$\vec{X} = \begin{pmatrix} x \\ x' \\ z \\ z' \end{pmatrix}.$$

If this vector is known at a coordinate s_0, $\vec{X}(s_0)$ can be transformed into $\vec{X}(s_1)$ by the corresponding transfer matrix M:

$$\vec{X}(s_1) = M \cdot \vec{X}(s_0).$$

Since the motions in the horizontal and vertical planes are independent of one another, this 4×4 matrix is block-diagonal and consists of two 2×2 matrices. Each element along the beamline can be described by a corresponding matrix:

- For a **drift** of length L, this 2×2 matrix is the same for the vertical and horizontal case

$$M_x^{\text{drift}} = M_z^{\text{drift}} = \begin{pmatrix} 1 & L \\ 0 & 1 \end{pmatrix}. \tag{3.8}$$

- In contrast, a single **quadrupole magnet** focuses the beam in one plane and defocuses it in the other plane. This corresponds to the quadrupole strengths k having opposite signs in each plane. $k > 0$ denotes the focusing case in the horizontal plane. For a quadrupole magnet with an effective length L, if one applies an approximation for short lengths, the transfer matrix is given by

$$M_x^{\text{Q}} = \begin{pmatrix} 1 & 0 & 0 & 0 \\ -kL & 1 & 0 & 0 \\ 0 & 0 & 1 & 0 \\ 0 & 0 & kL & 1 \end{pmatrix} \tag{3.9}$$

  In the analogy to geometrical optics, this corresponds to a thin lens with a focal length of $f = \frac{1}{kL}$.

- A **corrector magnet** will change the angle by an additional kick angle α without altering the displacement. However, this cannot be described by a matrix. In the experiment, we aim to choose this kick angle in such a way that it compensates for Earth's magnetic field and any other disturbances. If this is successfully achieved, we can describe the corrector magnet by a drift matrix whose length corresponds to the magnet's physical length.

The transfer matrix of a beamline is the product of the matrices corresponding to the elements along the beamline. The order in which the particle encounters the elements corresponds to the order of the matrices from right to left.

3.3.3. Emittance and Twiss Parameters

A beam is composed of the trajectories of all individual particles. The amplitude corresponding to one standard deviation σ of the particle distribution defines the envelope $E(s) = \sqrt{\epsilon\beta(s)}$. The emittance ϵ is a conserved quantity that characterizes the beam's focusing properties. $\beta(s)$ is one of the three Twiss parameters α, β, and γ.

These parameters also appear when considering the beam's phase space (x, x'). Here the values of particles at one standard deviation of the distribution are found on an ellipse, which encloses a constant area of $\pi\epsilon$. This is shown in Figure 3.8, which also shows that $\beta(s)$ is related to the beam width, $\gamma(s)$ describes the the angular width and $\alpha(s)$ expresses their correlation. The individual parameters are connected by the relations

$$\alpha(s) = -\frac{\beta'(s)}{2} \qquad \gamma(s) = \frac{1 + \alpha^2(s)}{\beta(s)} \tag{3.10}$$

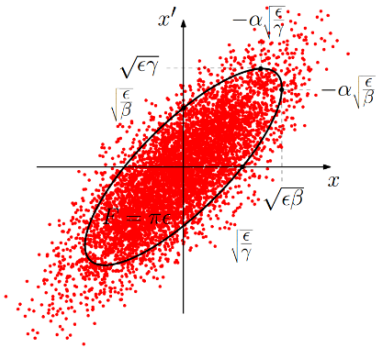

Figure 3.8.: Phase space ellipse in the horizontal plane. Figure taken from [1].

Using the Twiss parameters, the phase space ellipse equation reads

$$\epsilon = \gamma_x(s)x_i^2(s) + 2\alpha_x(s)x_i(s)x_i'(s) + \beta_x(s)x_i'^2(s). \tag{3.11}$$

The case for the vertical plane is analogous. Introducing the beta matrix

$$B_x(s) = \begin{pmatrix} \beta_x(s) & -\alpha_x(s) \\ -\alpha_x(s) & \gamma_x(s) \end{pmatrix} \tag{3.12}$$

the ellipse equation 3.11 can be expressed as

$$\epsilon = \vec{x}(s)^T \cdot B_x^{-1}(s) \cdot \vec{x}(s). \tag{3.13}$$

If the beta matrix at one coordinate $B_x(s_0)$ is known, its values at a different position s_1 can again be derived using the respective 2×2 transfer matrix M_x (for the horizontal case):

$$B_x(s_1) = M_x \cdot B_x(s_0) \cdot M_x^T \tag{3.14}$$

3.4. Quadrupole Scan

The aim of this part of the experiment is to calculate to the emittance ϵ using two different methods: the determinant method and the beam waist method.

3.4.1. Determining the Twiss Parameters

Method

The beam width σ at a screen Si can be expressed in terms of the Twiss parameters at the initial screen S0, the emittance ϵ and the transfer matrix elements m_{ij}. This is derived by evaluating the first component of the beta matrix $B(s)$ in equation 3.14 and multiplying with ϵ, as $\beta(s) \cdot \epsilon = \sigma^2$:

$$\sigma^2(k) = \beta\epsilon = m_{11}^2(k) \cdot (\epsilon\beta_0) - 2m_{11}(k) \cdot m_{12}(k) \cdot (\epsilon\alpha_0) + m_{12}^2(k) \cdot (\epsilon\gamma_0) \tag{3.15}$$

The transfer matrix elements are linearly dependent on the quadrupole strength k, thus we expect $\sigma^2(k)$ to be a parabola.

Measurement

In the experiment, we can set the quadrupole strength k by adjusting the quadrupole current I^Q and then measure the resulting beam width σ. We do this on two different screens, S1 and S2, and measure the beam width in both planes, σ_x and σ_z. We chose these screens because the beam appears to be better focused on the first screens.

The software directly translates the chosen quadrupole current into the corresponding quadrupole strength. We estimated the uncertainty of the quadrupole strength to be $0.1\,\mathrm{m}^{-2}$. This is based on the fluctuations we observed when using a fixed quadrupole current. Regarding the uncertainty of the beam width, the measured value fluctuates constantly. We read off a value in the middle of this fluctuation interval and take the maximum deviation we observed as its uncertainty. These values can be found in the Appendix in Tables A.13 and A.14.

Deriving the Transfer Matrix Elements

Using these measurements and fitting a parabola to them, we aim to determine $(\epsilon\alpha_0)$, $(\epsilon\beta_0)$ and $(\epsilon\gamma_0)$. To do so, we need to compute the transfer matrix elements for both screens. The transfer matrix can be written as the product of the individual matrices of the magnets and drifts involved. For the screen S1 the transfer matrix is:

$$M_{\mathrm{S1}} = M_{\text{half of S1}} \cdot M_{\text{drift 3}} \cdot M_{\mathrm{C1}} \cdot M_{\text{drift 2}} \cdot M_{\mathrm{Q1}} \cdot M_{\text{drift 1}} \cdot M_{\mathrm{S0}} \cdot M_{\text{drift 0}} \cdot M_{\mathrm{C0}}.$$

As the matrices are composed of 2×2 block matrices, the x and z direction can be computed separately. For all elements except for the quadrupole magnets the matrix is given as a drift with the element's physical length. The lengths L of the elements along the beamline are listed in the Appendix in Tables A.1 and A.2. For the quadrupole magnets, we use the effective length listed in Table A.2. This is the only part that is different in the vertical and horizontal direction, as the signs of k are opposite. However we will treat this as $k_x = -k_z$,

thus the change in sign is not included in matrix. Thus, up to the point of inserting concrete values for k, the matrices in both planes are the same. For the matrix calculations we use `python`'s computer algebra library `sympy`. The results are:

$$M_{\mathrm{S1}}(k) = \begin{pmatrix} 1 - 0.03300 \cdot k & 0.8137 - 0.01204 \cdot k \\ -0.074 \cdot k & 1 - 0.02701 \cdot k \end{pmatrix} \tag{3.16}$$

Analogously, the transfer matrix for S2 is given as

$$\begin{aligned} M_{\mathrm{S2}} = M_{\text{half of S2}} \cdot M_{\text{drift 6}} \cdot M_{\mathrm{C2}} \cdot M_{\text{drift 5}} \cdot M_{\mathrm{Q2}} \cdot M_{\text{drift 4}} \cdot M_{\mathrm{S1}} \cdot M_{\text{drift 3}} \cdot M_{\mathrm{C1}} \\ \cdot M_{\text{drift 2}} \cdot M_{\mathrm{Q1}} \cdot M_{\text{drift 1}} \cdot M_{\mathrm{S0}} \cdot M_{\text{drift 0}} \cdot M_{\mathrm{C0}}. \end{aligned}$$

For this second measurement the first quadrupole magnet is turned off. Therefore it is also described by a drift matrix with its physical length. Again, using the values for the lengths from the script listed in Tables A.1 and A.2 yields:

$$M_{\mathrm{S2}}(k) = \begin{pmatrix} 1 - 0.03300 \cdot k & 1.411 - 0.03184 \cdot k \\ -0.074 \cdot k & 1 - 0.07141 \cdot k \end{pmatrix} \tag{3.17}$$

Fit Procedure

We measured the width σ, but the fit will be performed for σ^2, thus using Gaussian error propagation the uncertainty is

$$\Delta\sigma^2 = 2\sigma\Delta\sigma.$$

We fit a parabola

$$\sigma^2(k) = ak^2 + bk + c \tag{3.18}$$

to our data. The results are shown in Figure 3.9, including the fit parameters.

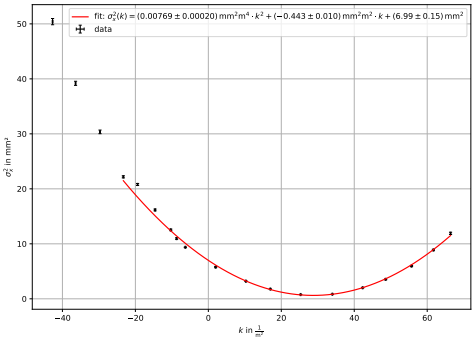

(a) Fit for the Quadrupole Scan at screen S1, horizontal direction. $\chi^2/\mathrm{ndf} = 31.75$

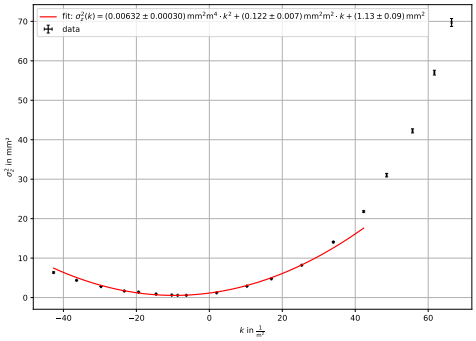

(b) Fit for the quadrupole scan at screen S1, vertical direction. $\chi^2/\mathrm{ndf} = 99.82$

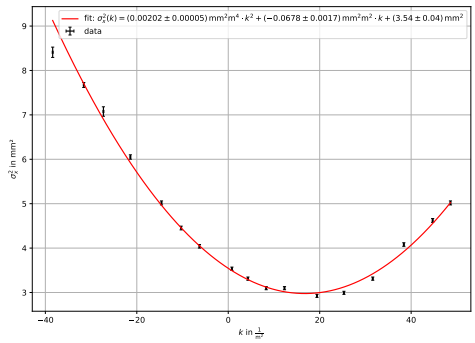

(c) Fit for the quadrupole scan at screen S2, horizontal direction. $\chi^2/\mathrm{ndf} = 7.29$

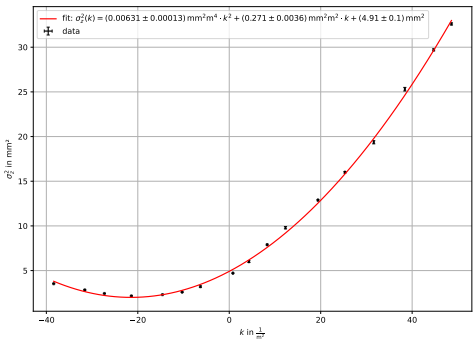

(d) Fit for the quadrupole scan at screen S2, vertical direction. $\chi^2/\mathrm{ndf} = 28.27$

Figure 3.9.: Quadrupole scan at Screens S1 and S2 for both planes: squared beam width σ as a function of the quadrupole strength k.

For these two measurements, we used fairly high quadrupole strengths. We suspect that for values far from the minimum of the parabola, a linear relation may better describe the relationship between the squared beam width and the quadrupole strength. Our measurement interval is distributed asymmetrically around the minimum for both planes. In both cases, the values far from the minimum deviated significantly from the fitted parabola. Thus, we decided to exclude the outermost values from the fit. These values are still included in the plot, however, the fit is only shown over the range of values that were actually used. Additionally, these values are highlighted in Table A.13.

Now, if the left-hand side of Eq. 3.15 is rearranged in powers of k, the resulting coefficients correspond to the fit parameters. First, consider the quadrupole scan at screen S1. Inserting the transfer matrix elements into Eq. 3.15 gives:

$$
\begin{aligned}
a &= -0.000\,802\,9\,\mathrm{m}^5(\epsilon\alpha_0) + 0.001\,096\,\mathrm{m}^4(\epsilon\beta_0) + 0.000\,147\,1\,\mathrm{m}^6(\epsilon\gamma_0) \\
b &= 0.078\,13\,\mathrm{m}^3(\epsilon\alpha_0) - 0.066\,21\,\mathrm{m}^2(\epsilon\beta_0) - 0.019\,73\,\mathrm{m}^4(\epsilon\gamma_0) \\
c &= -1.627\,\mathrm{m}(\epsilon\alpha_0) + (\epsilon\beta_0) + 0.6621\,\mathrm{m}^2(\epsilon\gamma_0)
\end{aligned}
$$

Now consider the quadrupole scan at screen Q2. This yields

$$
\begin{aligned}
a &= -0.002\,124\,\mathrm{m}^5(\epsilon\alpha_0) + 0.001\,096\,\mathrm{m}^4(\epsilon\beta_0) + 0.001\,029\,\mathrm{m}^6(\epsilon\gamma_0) \\
b &= 0.1579\,\mathrm{m}^3(\epsilon\alpha_0) - 0.066\,21\,\mathrm{m}^2(\epsilon\beta_0) - 0.090\,87\,\mathrm{m}^4(\epsilon\gamma_0) \\
c &= -2.833\,\mathrm{m}(\epsilon\alpha_0) + (\epsilon\beta_0) + 2.006\,\mathrm{m}^2(\epsilon\gamma_0).
\end{aligned}
$$

This is then solved for $(\epsilon\alpha_0)$, $(\epsilon\beta_0)$ and $(\epsilon\gamma_0)$ using `sympy`. For the uncertainties we apply Gaussian error propagation to the relations we found, again using `sympy`. The results are listed in Table 3.2.

Table 3.2.: Results for $(\epsilon\alpha_0), (\epsilon\beta_0)$ and $(\epsilon\gamma_0)$ for all quadrupole scans.

	$(\epsilon\alpha_0)$ / mm^{2}m^{-1}	$(\epsilon\beta_0)$ / mm^2	$(\epsilon\gamma_0)$ / mm^{2}m^{-2}
Q1 x	1.9(12)	7.97(76)	3.1(19)
Q1 z	36.4(13)	25.33(96)	52.8(18)
Q2 x	17.98(49)	21.04(61)	16.67(94)
Q2 z	15.7(12)	24.6(15)	1.48(95)

3.4.2. Emittance via the Determinant

To determine the emittance from $(\epsilon\alpha_0)$, $(\epsilon\beta_0)$ and $(\epsilon\gamma_0)$ we can use the relation

$$
\det(B) = \beta\gamma - \alpha^2 = 1 + \alpha^2 - \alpha^2 = 1 \quad \Longrightarrow \quad (\epsilon\gamma_0)\cdot(\epsilon\beta_0) - (\epsilon\alpha_0)^2 = \epsilon^2. \tag{3.19}
$$

And thus, using Gaussian error propagation we get

$$
\begin{aligned}
\epsilon &= \sqrt{(\epsilon\gamma_0)\cdot(\epsilon\beta_0) - (\epsilon\alpha_0)^2} \\
\Delta\epsilon &= \sqrt{\left(\frac{\Delta(\epsilon\alpha_0)\cdot(\epsilon\alpha_0)}{\epsilon}\right)^2 + \left(\frac{\Delta(\epsilon\beta_0)\cdot(\epsilon\gamma_0)}{2\epsilon}\right)^2 + \left(\frac{\Delta(\epsilon\gamma_0)\cdot(\epsilon\beta_0)}{2\epsilon}\right)^2}
\end{aligned}
$$

Inserting the values for $(\epsilon\alpha_0)$, $(\epsilon\beta_0)$ and $(\epsilon\gamma_0)$ we determined from the fit, we obtain the following results for the emittance (see Table 3.3):

Table 3.3.: Emittances determined using the determinant method

	x	z
Q1	4.6(14) mm mrad	3.95(45) mm mrad
Q2	5.23(9) mm mrad	7.59(31) mm mrad

3.4.3. Emittance via the Beam Waist

An alternative way to determine the emittance is by using the equation for γ in the beta matrix (again derived from Equation 3.14):

$$
\gamma_1 = m_{21}^2\beta_0 - 2m_{21}\cdot m_{22}\cdot\alpha_0 + m_{22}^2\gamma_0. \tag{3.20}
$$

As $\beta(w)$ is extremal at the waist w, $\alpha(w) = -\frac{\beta'(w)}{2} = 0$ and $\gamma(w) = \frac{1+\alpha^2(w)}{\beta(w)} = \frac{1}{\beta(w)}$. Thus multiplying this equation with ϵ yields

$$\epsilon^2 = \sigma^2(w) \left[m_{21}^2(s, k_w) \cdot (\epsilon\beta_0) - 2m_{21}(s, k_w) \cdot m_{22}(s, k_w) \cdot (\epsilon\alpha_0) + m_{22}^2(\epsilon\gamma_0) \right]. \tag{3.21}$$

Here the beam waist w corresponds to the minimum of the parabola $\sigma^2(k)$, which we can extrapolate from out fit parameters as

$$k(w) = -\frac{b}{2a} \qquad \Delta k(w) = \sqrt{\left(\frac{\Delta b}{2a}\right)^2 + \left(\frac{b\Delta a}{2a^2}\right)^2}$$

This way we find the values at the beam waist listed in Table 3.4. These are inserted into

Table 3.4.: Quadrupole strengths at the beam waist

	k_w / m^{-2}
Q1 x	28.80(75)
Q1 z	9.65(60)
Q2 x	16.78(47)
Q2 z	21.47(36)

Equation 3.21 using `sympy`. The error propagation is done using gaussian error propagation for the relations found with `sympy`. The results for the emittance using the beam waist method are given in Table 3.5.

Table 3.5.: Emittances determined using the beam waist method

	x	z
Q1	2.735(69) mm mrad	0.650(40) mm mrad
Q2	0.333(8) mm mrad	1.687(26) mm mrad

3.5. Multi-screen Method

The multi-screen method is an alternative to the quadrupole scan method for determining the emittance-scaled Twiss parameters $(\epsilon\alpha_0)$, $(\epsilon\beta_0)$ and $(\epsilon\gamma_0)$. Once these values have been evaluated, either the determinant method or the beam waist method can be applied to derive the emittance.

3.5.1. Method

This approach is again based on Eq. 3.15, however in contrast to the quadrupole scan, we will take measurements at different screens s_i instead of varying the quadrupole strength k. This leads to the following set of equations

$$\underbrace{\begin{pmatrix}\sigma^2(s_0)\\ \sigma^2(s_1)\\ \sigma^2(s_2)\\ \sigma^2(s_3)\\ \sigma^2(s_4)\end{pmatrix}}_{=\vec{\sigma}} = \underbrace{\begin{pmatrix}m_{11}^2(s_0) & -2m_{11}(s_0)\cdot m_{12}(s_0) & m_{12}^2(s_0)\\ m_{11}^2(s_1) & -2m_{11}(s_1)\cdot m_{12}(s_1) & m_{12}^2(s_1)\\ m_{11}^2(s_2) & -2m_{11}(s_2)\cdot m_{12}(s_2) & m_{12}^2(s_2)\\ m_{11}^2(s_3) & -2m_{11}(s_3)\cdot m_{12}(s_3) & m_{12}^2(s_3)\\ m_{11}^2(s_4) & -2m_{11}(s_4)\cdot m_{12}(s_4) & m_{12}^2(s_4)\end{pmatrix}}_{=\mathcal{M}} \cdot \underbrace{\begin{pmatrix}\epsilon\beta_0\\ \epsilon\alpha_0\\ \epsilon\gamma_0\end{pmatrix}}_{=\vec{x}}. \tag{3.22}$$

By multiplying with $\mathcal{M}^T$ from the left, the system of five equations above can be transformed into a set of three equations:

$$\mathcal{M}^T\cdot\vec{\sigma} = \left(\mathcal{M}^T\cdot\mathcal{M}\right)\cdot\vec{x}, \tag{3.23}$$

This can be solved for $\vec{x}$ to determine $(\epsilon\alpha_0)$, $(\epsilon\beta_0)$ and $(\epsilon\gamma_0)$.

3.5.2. Measurement

In order to evaluate the equations introduced above, we measure the beam width σ in the x and z directions at all five screens. We choose the quadrupole strength k such that the beam is as focused as possible, while alternating signs, and then keep it fixed at this value.

Table 3.6.: Quadrupole strengths chosen for the multi-screen measurement

	Q1	Q2	Q3	Q4
$k\,/\,\mathrm{m}^{-2}$	14.6(1)	−17.0(1)	38.4(1)	−40.7(1)

The uncertainties are estimated analogously to the quadrupole scan measurement in Section 3.4.1. The values for the quadrupole strengths are listed in Table 3.6 and the measurements for the beam widths on each screen can be found in Table 3.7.

To use the beam waist method, we would have had to adjust the beam in such a way that one of the screens was placed at the beam waist. We did not do this, therefore, to find the emittance, we will use the determinant method.

3.5.3. Evaluation of the Measurement

The values for the squared beam widths and their uncertainties are listed in Table 3.7.

Table 3.7.: Measured values for the beam widths σ_x and σ_y on all screens as well as their uncertainties.

	S0	S1	S2	S3	S4
σ_x / mm	2.17(3)	1.49(2)	2.35(2)	1.64(2)	4.14(3)
σ_x^2 / mm^2	4.71(13)	2.22(6)	5.52(9)	2.69(7)	17.14(25)
σ_y / mm	2.14(3)	1.99(1)	1.56(2)	3.78(2)	1.15(1)
σ_y^2 / mm^2	4.58(13)	3.96(4)	2.43(6)	14.29(15)	1.32(23)

The evaluation of these values is performed by solving the linear system of Eq. 3.23 using `sympy`. The transfer matrix elements at the different screens are computed analogously to those in the quadrupole scan method described in Section 3.4.1, but this time by inserting each quadrupole strength k listed in Table 3.6.

The values obtained for $(\epsilon\alpha_0)$, $(\epsilon\beta_0)$ and $(\epsilon\gamma_0)$ using this method are listed in Table 3.8. The errors were again computed using Gaussian error propagation.

Table 3.8.: Results for $(\epsilon\alpha_0)$, $(\epsilon\beta_0)$ and $(\epsilon\gamma_0)$ for the multi-screen method.

	$(\epsilon\alpha_0)$ / mm^{2}m^{-1}	$(\epsilon\beta_0)$ / mm^2	$(\epsilon\gamma_0)$ / mm^{2}m^{-2}
x direction	−0.25(18)	4.01(19)	2.396(75)
z direction	9.04(31)	8.89(27)	11.15(35)

After applying the determinant method, the resulting emittances are:

$$\epsilon_x = 1.78(43)\,\text{mm mrad} \qquad \epsilon_z = 4.156(48)\,\text{mm mrad}$$

3.6. Comparison of the Emittance Values

In the previous two sections, various measurement and analysis methods were used to determine the beam emittance. The emittances obtained from the quadrupole scan are listed in Table 3.9.

Table 3.9.: Overview of the emittances determined via the quadrupole scan

	determinant method		beam waist method	
	Q1	Q2	Q1	Q2
ϵ_x / mm mrad	4.6(14)	5.23(9)	2.735(69)	0.333(8)
ϵ_z / mm mrad	3.95(45)	7.59(31)	0.650(40)	1.687(26)

The emittances calculated using the multi-screen method are

$$\epsilon_x = 1.78(43)\,\text{mm mrad} \qquad \epsilon_z = 4.156(48)\,\text{mm mrad}.$$

Fundamentally, all values lie within a range typical for accelerators - on the order of a few mm mrad. However, the differences between the values are large and, in some cases, significantly exceed the respective error intervals. The most likely reason for this and one of the main sources of error is the shape of the electron beam. For determining the beam width, the software assumes that the beam profile is Gaussian, which is not always the case, particularly when adjusting the quadrupoles. Therefore, we must assume that systematic errors play a major role in the quadrupole scan and dominate over the statistical error. Otherwise, the strong deviations between the emittance values cannot be explained. Consequently, we would place more trust in the values determined by the multi-screen method, since in that case the quadrupoles were adjusted so that the beam was well focused everywhere and the beam width was therefore likely determined more reliably. However, even in this case, possible sources of error include poor beam alignment or inaccuracies of the screens.

4. Conclusion

Particle accelerators play a very important role in modern science and medicine. Through this experiment at the 25 keV LAB accelerator, we gained a better understanding of an accelerator's functionality and characteristic quantities, and in particular, we appreciated how important and intricate proper alignment and focusing of the beam are.

In the first part of the experiment, we examined the calibration of two of the corrector magnets. We were able to ascertain the expected linear relationship between the applied kick angle and the measured beam displacement. However, the experimentally determined slope for this relationship (corresponding to the distance between the corrector and the screen) was invariably higher than the actual values. This indicates the occurrence of a systematic error or a miscalibration of the corrector magnets used.

After that, the beam was aligned so that it passed through the center of each quadrupole magnet. For this purpose, the corrector placed in front of each quadrupole had to be adjusted appropriately. The optimal corrector angles in both the horizontal and vertical planes were determined by a linear fit.

Once the beam was well aligned, its emittance was determined using two different methods. For the quadrupole scan, the strength of two quadrupoles was varied and the resulting beam spread in the horizontal and vertical directions was measured. In contrast, for the multiscreen method the quadrupole strengths were adjusted such that the beam was as focused as possible and the width was measured at the five different screens.

Both the quadrupole scan and the multiscreen method allow for determining values for the emittance-scaled Twiss parameters $\epsilon\alpha$, $\epsilon\beta$ and $\epsilon\gamma$. The emittance can then be determined either via the determinant of the beta matrix or via the beam waist method. For the quadrupole scan, both methods were used, whereas for the multiscreen method only the determinant was applicable, since the position of the beam waist was not determined.

The resulting emittance values sometimes differ significantly from one another, but they all lie in the range of a few mm mrad, which is consistent with expectations. The deviations are most likely primarily due to the beam profile, which in some cases appears very different and complicates the determination of the beam width.

A. Appendix

A.1. Verification of the Corrector Magnet Calibration

Table A.1.: Values for the displacement x and z as a function of the applied angle α for the corrector magnet C0.

α_x / °	x / mm
−70.0(1)	−9.08(2)
−65.2(1)	−7.83(2)
−60.3(1)	−6.54(3)
−55.1(1)	−5.12(2)
−50.2(1)	−3.75(2)
−45.3(1)	−2.43(3)
−40.4(1)	−1.05(2)
−34.6(1)	0.62(2)
−30.4(1)	1.85(2)
−24.6(1)	3.59(2)
−19.8(1)	5.04(2)
−14.0(1)	6.73(2)
−9.9(1)	7.98(2)

(a) Angles and displacements in horizontal direction

α_z / °	z / mm
−39.5(1)	−6.22(2)
−34.6(1)	−4.85(2)
−30.4(1)	−3.58(3)
−24.6(1)	−1.84(2)
−19.8(1)	−0.43(2)
−14.8(1)	1.19(3)
−9.8(1)	2.84(3)
−4.7(1)	4.43(2)
0.2(1)	5.83(2)
5.6(1)	7.39(3)

(b) Angles and displacements in vertical direction

Table A.3.: Values for the displacement x and z as a function of the applied angle α for the corrector magnet C1.

α_x / °	x / mm
−34.6(1)	−11.04(3)
−29.6(1)	−9.30(3)
−24.6(1)	−7.55(3)
−19.8(1)	−5.71(3)
−14.8(1)	−3.00(3)
−9.8(1)	−0.54(3)
−4.7(1)	1.85(3)
0.8(1)	4.73(3)
5.6(1)	6.93(2)
10.5(1)	9.07(3)

(a) Angles and displacements in horizontal direction

α_z / °	z / mm
9.0(1)	−8.47(3)
14.0(1)	−6.61(3)
19.8(1)	−3.62(4)
24.6(1)	0.22(3)
29.6(1)	3.22(2)
34.6(1)	5.55(3)
39.5(1)	7.66(1)
44.7(1)	9.31(2)

(b) Angles and displacements in vertical direction

A.2. Beam-based Alignment

Table A.5.: Measurements for the beam-based alignment of the corrector magnet C0 in x and z direction.

I^C / A	x_1 / mm	x_2 / mm	Δx / mm
−0.1430(5)	−4.44(4)	−8.66(4)	4.22(6)
−0.1270(5)	−0.68(4)	−3.33(4)	2.65(6)
−0.1130(5)	2.91(4)	2.37(4)	0.54(6)
−0.1000(5)	6.14(4)	7.50(4)	−1.36(6)
−0.0890(5)	8.49(4)	10.86(4)	−2.37(6)

(a) Differences in the horizontal displacement

I^C / A	z_1 / mm	z_2 / mm	Δz / mm
−0.0730(5)	−7.47(5)	−1.70(5)	−5.77(7)
−0.0570(5)	0.78(5)	3.66(5)	−2.88(7)
−0.0430(5)	6.97(4)	7.38(4)	−0.41(6)
−0.0400(5)	8.08(3)	8.07(3)	0.01(4)
−0.0340(5)	9.81(3)	9.24(3)	0.57(4)

(b) Differences in the vertical displacement

Table A.7.: Measurements for the beam-based alignment of the corrector magnet C1 in x and z direction.

I^C / A	x_1 / mm	x_2 / mm	Δx / mm
−0.0590(5)	−2.45(4)	−4.45(8)	2.00(9)
−0.0540(5)	0.03(6)	−0.64(10)	0.67(12)
−0.0510(5)	1.19(5)	1.30(6)	−0.11(8)
−0.0460(5)	3.82(3)	5.36(4)	−1.54(5)
−0.0400(5)	6.50(5)	9.53(5)	−3.03(7)

(a) Differences in the horizontal displacement

I^C / A	z_1 / mm	z_2 / mm	Δz / mm
0.0320(5)	−5.61(3)	2.17(3)	−7.78(4)
0.0430(5)	0.05(4)	3.04(4)	−2.99(6)
0.0560(5)	4.41(3)	4.11(3)	0.30(4)
0.0620(5)	6.01(4)	4.48(4)	1.53(6)
0.0680(5)	8.11(4)	4.91(3)	3.20(5)

(b) Differences in the vertical displacement

Table A.9.: Measurements for the beam-based alignment of the corrector magnet C2 in x and z direction.

I^C / A	x_1 / mm	x_2 / mm	Δx / mm
−0.1290(5)	3.36(4)	−6.50(5)	9.86(6)
−0.1070(5)	2.96(6)	−0.55(7)	3.51(9)
−0.0940(5)	3.03(3)	3.44(6)	−0.41(7)
−0.0800(5)	2.92(4)	7.20(4)	−4.28(6)
−0.0700(5)	2.71(3)	9.95(6)	−7.24(7)

(a) Differences in the horizontal displacement

I^C / A	z_1 / mm	z_2 / mm	Δz / mm
0.0760(5)	−1.59(5)	−2.84(4)	1.25(6)
0.0790(5)	0.94(4)	−1.36(4)	2.30(6)
0.0810(5)	2.70(4)	−0.22(3)	2.92(5)
0.0840(5)	4.95(5)	1.30(4)	3.65(6)

(b) Differences in the vertical displacement

Table A.11.: Measurements for the beam-based alignment of the corrector magnet C3 in x and z direction.

I^C / A	x_1 / mm	x_2 / mm	Δx / mm
−0.1050(5)	2.24(10)	−2.00(6)	4.24(12)
−0.1000(5)	5.16(6)	1.99(10)	3.17(12)
−0.0970(5)	6.39(5)	4.0(1)	2.39(11)
−0.0920(5)	9.45(10)	8.07(8)	1.38(13)
−0.0890(5)	10.80(4)	10.16(6)	0.64(7)

(a) Differences in the horizontal displacement

I^C / A	z_1 / mm	z_2 / mm	Δz / mm
0.0340(5)	−4.09(5)	0.05(4)	−4.14(6)
0.0430(5)	−2.65(5)	0.09(4)	−2.74(6)
0.0530(5)	−0.95(4)	0.3(1)	−1.25(11)
0.0650(5)	1.02(4)	0.51(4)	0.51(6)
0.0750(5)	2.63(5)	0.47(4)	2.16(6)

(b) Differences in the vertical displacement

A.3. Quadrupole Scan

Table A.13.: Quadrupole scan for Q1: Beam width σ in both x and z direction as a function of the quadrupole strength k. The values marked with * were not included in the respective fit of this data. The value for k corresponds to the strength in the horizontal plane, the one in the vertical plane has the opposite sign.

I^Q / A	k / m^{-2}	σ_x / mm	σ_z / mm
−0.054(1)	−42.7(1)]	7.10(4)*	2.52(3)
−0.037(1)	−29.7(1)	5.51(3)*	1.67(1)
−0.046(1)	−36.4(1)	6.26(3)*	2.09(2)
−0.030(1)	−23.3(1)	4.71(2)	1.29(1)
−0.024(1)	−19.4(1)	4.56(2)	1.18(1)
−0.019(1)	−14.6(1)	4.02(2)	0.94(1)
−0.013(1)	−10.3(1)	3.54(2)	0.79(1)
−0.011(1)	−8.7(1)	3.31(2)	0.75(1)
−0.008(1)	−6.3(1)	3.06(1)	0.75(1)
0.003(1)	2.0(1)	2.40(2)	1.10(1)
0.013(1)	10.3(1)	1.79(2)	1.70(1)
0.022(1)	17.0(1)	1.33(1)	2.18(1)
0.032(1)	25.3(1)	0.88(2)	2.86(1)
0.043(1)	34.0(1)	0.91(2)	3.75(2)
0.053(1)	42.3(1)	1.42(2)	4.67(2)
0.062(1)	48.6(1)	1.88(2)	5.57(4)*
0.070(1)	55.7(1)	2.44(2)	6.50(4)*
0.078(1)	61.7(1)	2.98(2)	7.55(4)*
0.084(1)	66.4(1)	3.45(3)	8.35(6)*

Table A.14.: Quadrupole scan for Q2: Beam width σ in both x and z direction as a function of the quadrupole strength k. The value for k corresponds to the strength in the horizontal plane, the one in the vertical plane has the opposite sign.

I^Q / A	k / m^{-2}	σ_x / mm	σ_z / mm
−0.049(1)	−38.4(1)	2.90(2)	1.88(1)
−0.040(1)	−31.6(1)	2.77(1)	1.68(2)
−0.034(1)	−27.3(1)	2.66(2)	1.56(1)
−0.027(1)	−21.4(1)	2.46(1)	1.47(1)
−0.019(1)	−14.6(1)	2.24(1)	1.52(1)
−0.013(1)	−10.3(1)	2.11(1)	1.61(1)
−0.008(1)	−6.3(1)	2.01(1)	1.79(2)
0.001(1)	0.8(1)	1.88(1)	2.17(1)
0.006(1)	4.3(1)	1.82(1)	2.45(2)
0.010(1)	8.3(1)	1.76(1)	2.81(1)
0.016(1)	12.3(1)	1.76(1)	3.13(2)
0.024(1)	19.4(1)	1.71(1)	3.59(1)
0.032(1)	25.3(1)	1.73(1)	4.00(1)
0.040(1)	31.6(1)	1.82(1)	4.40(2)
0.049(1)	38.4(1)	2.02(1)	5.03(2)
0.056(1)	44.7(1)	2.15(1)	5.45(1)
0.062(1)	48.6(1)	2.24(1)	5.71(1)

name	type	length / m
C0	corrector	0.0785
	drift	0.185
S0	screen	0.04
	drift	0.06
Q1	quadrupole	0.074
	drift	0.03
C1	corrector	0.0785
	drift	0.316
S1	screen	0.04
	drift	0.06
Q2	quadrupole	0.074
	drift	0.03
C2	corrector	0.0785
	drift	0.316
S2	screen	0.04
	drift	0.06
Q3	quadrupole	0.074
	drift	0.03
C3	corrector	0.0785
	drift	0.316
S3	screen	0.04
	drift	0.06
Q4	quadrupole	0.074
	drift	0.03
C4	corrector	0.0785
	drift	0.316
S4	screen	0.04

Figure A.1.: Lengths of all elements of the LAB experiment and drift spaces between them. Taken from the LAB script [1].

Corrector Parameters

coil geometry	round
coil radius	40 mm
number of windings	300 (in 8 layers)
coil distance	105 mm
wire diameter	0.3 mm
physical length L_{phys}	80 mm
effective field length L_{eff}	78.5 mm

Quadrupole Parameters

coil geometry	rectangular
coil edge length	52 mm × 72 mm
number of windings	120 (in 4 layers)
half aperture a	28 mm
wire diameter	0.3 mm
physical length L_{phys}	(71.3 ± 0.5) mm
effective field length L_{eff}	(74 ± 1) mm

Figure A.2.: Parameters of the quadrupole and corrector magnets, taken from the LAB script [1].

List of Figures

List of Tables

Bibliography

[1] Physikalisches Institut der Universität Bonn. *Lab Course Accelerator Bonn (LAB)*. February 2020.